Data-Driven Power System Linear Model Identification via Quadrature-Based Balanced Truncation

Mario. R. Arrieta Paternina, *Member, IEEE*, José A. Moreno-Corbea, *Student Member, IEEE*, Juan M. Ramirez, *Member, IEEE*, Joe H. Chow, *Life Fellow, IEEE*, and Alejandro Zamora-Mendez, *Member, IEEE*

***Abstract*—This paper introduces the novel formulation of the quadrature-based balanced truncation (QBBT) method to identify large-scale power system linear models precisely. The QBBT interpolates a directional frequency dataset that is extracted from a dynamic system, by following a quadrature rule to be applied from weighted data for deriving a linear system model based on approximations of Gramians and providing an alternative approach to the balanced truncation (BT) formulation that makes use of the system model. In this investigation, an accurate theoretical framework is presented to achieve the application of QBBT considering power systems as black-box models. The Boyd/Clenshaw-Curtis (BCC) quadrature rule is implemented by using different adjustments to identify linear models of different order. The attained results and their validation with analytical power system models confirm the method's potential to retail oscillatory dynamics. The QBBT's effectiveness is compared with the Loewner-based frequency interpolation (LBFI) approach and the BT method on the Klein-Rogers-Kundur (KRK) benchmark power system and the equivalent of the New England transmission system - New York power system (NETS-NYPS), achieving a small absolute error in the magnitude of the frequency response of the models of the order of 1×10^{-3} dB in comparison with other state-of-the-art methods.**

Link to graphical and video abstracts, and to code: https://latamt.ieeer9.org/index.php/transactions/article/view/9597

***Index Terms*—Balanced truncation, quadrature rules, system identification, directional frequency dataset, power system linear model.**

I. Introduction

MODERN power systems are large and complex dynamic systems formed by physical components that are challenging to characterize [1]. Linear models of power systems constitute valuable representations that provide key information about the oscillatory dynamics that can cause instabilities [1], [2]; they are also fundamental for the analysis of small-signal stability [3]. Given that the power systems' growth increases their complexity, appropriate tools are essential to perform the small-signal analysis (SSA).

Large-scale power systems are highly nonlinear dynamic systems due to the large number of non-linear components that make them up, such as generators, controllers, nonlinear loads, transmission lines, etc. Traditionally, power system linear models are analytically derived by linearizing the set of differential-algebraic equations (DAE) that describe their dynamic behavior [4], [5]. To achieve this linearization, the Taylor series expansion is employed by neglecting the higher-order terms [5], or perturbing the nonlinear model to solve the aforementioned expansion numerically [6]. When power system linear models are derived using these approaches, the system swing modes are studied considering that the precise knowledge of the power system components' parameters [7] is available, which is not always available. Thus, these approaches provide linear models with a large number of state variables, constituting problems regarding their application.

To provide a solution to the large number of states resulting in the linear models obtained through linearization (analytical or numerical), the balanced realization proposed by Bruce Moore in [8] was successfully introduced into power systems. This concept allowed the balanced truncation (BT) of the non-controllable and non-observable states of the systems, making use of the controllability and observability Gramians that respectively correspond to matrices for defining the optimal inputs to control the states and the optimal outputs to observe them. BT is a reduction order-model (ROM) technique that requires access to the linear model matrices. Its application in power systems has allowed researchers to obtain a low-dimensional linear model with a high reduction rate [9].

The system identification techniques applied in power systems to obtain linear models explicitly as state-space models (SSM) or transfer functions, can be grouped into two fundamental approaches according to the nature (known or non-intentional) of the input signals in the identification process [10]. These approaches correspond to probing signals methods [11], [12], which deal with applying known signals to the system inputs and measuring their outputs; and the transient data analysis-based methods that are applied to power systems

The associate editor coordinating the review of this manuscript and approving it for publication was Gabriel Pinto (*Corresponding author: Alejandro Zamora-Mendez*).

M. R. A. Paternina and J. A. Moreno-Corbea are with the Department of Electrical Engineering, National Autonomous University of Mexico, Mexico City, Mexico (e-mails: jamcorbea@comunidad.unam.mx, and mra.paternina@fi-b.unam.mx).

J. M. Ramirez is with the Department of Electrical Engineering at CINVESTAV, Guadalajara, Mexico (e-mail: joramirez@cinvestav.mx).

J. H. Chow is with the Department of Electrical, Computer and Systems Engineering, Rensselaer Polytechnic Institute, Troy, NY, 12180-3590, USA (e-mail: chowj@rpi.edu).

A. Zamora is with the Electrical Engineering Faculty, at the Michoacan University of Saint Nicholas of Hidalgo, Morelia, Michoacan, Mexico (e-mail: azamoram@umich.mx).

after a disturbance exciting their oscillatory dynamics, and these are only based on measuring of the power system outputs [13].

Probing signals methods: As part of this approach, the Vector Fitting (VF) method is one of them, whose main disadvantages are that it is iterative, and that a poor selection of the initial location of the system poles can require numerous iterations to guarantee an accurate modal extraction of the power system. Also, the Chirp-based ERA algorithm was correctly applied in [14], modulating with Chirp signals the reactive and active reference power of battery chargers to identify accurate power system linear models, however the accuracy of the identified model is not explored. Another method is the Loewner-based frequency interpolation (LBFI) which obtain an SSM from a directional frequency dataset or also known as tangential interpolation data [15]. The LBFI method was introduced in power systems in [16] to obtain its linear model represented as an SSM in descriptor form. The authors in [17] and [18] applied the LBFI to identify linear models from large power systems in selected frequency ranges. Nevertheless, its application does not incorporate an error control criterion.

Transient data analysis: The authors in [19] obtain linear models using the Matrix Pencil (MP) technique [20], and the Eigensystem Realization Algorithm (ERA) [21], demonstrating that the MP has greater accuracy. Both MP and ERA constitute subspace methods, that make use of the singular value decomposition (SVD) [22], for determining appropriate system orders and capturing the most significant energy contained in the singular values. Also, these methods were applied to the ringdown analysis of selected system outputs, from events that excite their low-frequency dynamics and provoke undesired operating conditions [19], [23]. Furthermore, the numerical algorithm for system identification (N4SID) was used to identify an accurate linear model of the Western Electricity Coordinating Council (WECC) from time-domain signals [24].

Obtaining accurate models is a premise in the identification process, and this characteristic is achieved to a greater extent in techniques based on the probing signals methods where the frequency interpolation process improves the system identification [16]–[18]. Methods such as N4SID, MP, ERA, VF, and LBFI use the SVD, making it possible to obtain linear representations in which there is control over the number of state variables that describe the system. Thus, one of the key needs lies in deriving accurate linear models that benefit the tuning of local or global system controllers.

Recently, the Quadrature-Based Balanced Truncation (QBBT) method was proposed in [25], where the authors developed and demonstrated a new formulation based on the classical BT model reduction technique, but they approximate the controllability and observability Gramians using quadrature rules instead of the analytical linear models. From these approximations and interpolating weighted directional frequency data, an accurate linear model can be obtained in comparison with the ROM technique based on BT, but without requiring explicit access to the model. Numerical results were reported in [25], working from frequency dataset and extracting the model from transfer functions of dynamical systems using the Boyd/Clenshaw-Curtis (BCC) quadrature rule.

According to the notable differences among the above-mentioned methods, Table I showcases a comparison among the main features, where each feature is marked by **X**. The characteristics were selected based on the type of data used for identification, the number of signals or channels, the mathematical foundations of the methods, and the provided representation.

The large-scale power systems and their complexity in modeling their oscillatory dynamics have turned the investigations to explore and develop techniques in a data-driven manner [13], [29]. For this perspective, power system linear models have been derived through different identification techniques that consider the power system as a black-box model, which is useful for the identification of electromechanical modes [13], tuning wide-area damping controllers [30], and coherent analysis [31]. One of the main challenges that face the system identification methods in power systems whether they are based on frequency data or time data, is the accuracy of the identified models [16]–[19], [32]. Where the reduced order in the identification process is a desired characteristic, as well as in analytical or numerical linearizations [33], [34]. Thus, the contribution in the state-of-the-art is to introduce the use of weighted data, regarding the identification of power system linear models. Thereby, the order and accuracy of linear models identified from weighted data are investigated in this research.

A. Contributions

The major contribution of this paper lies in proposing a methodology to identify the power system linear model through the non-intrusive QBBT method retaining the oscillatory dynamics of the full model. Thus, our contribution simultaneously solves two problems associated with system identification in power systems, which are accuracy and the rate of the reduction rate of models. The key contributions of this paper are summarized as follows:

- The QBBT is formulated and adopted to provide power system linear models, changing the traditional paradigm from BT to a data-driven technique.
- It proposes adjustments to the quadrature rule Boyd/Clenshaw-Curtis (BCC), which are associated with the number of points and the truncation constants in the approximations. Such adjustments guarantee accurate

TABLE I
COMPARISON OF FEATURES OF THE SYSTEM IDENTIFICATION METHODS APPLIED TO POWER SYSTEMS

Methods	Data		Weighted data	Iterative	System realization	Multi channel
	Time	Freq.				
N4SID [24]	**X**				**X**	**X**
MP [19], [20]	**X**				**X**	**X**
ERA [19], [23], [21]	**X**				**X**	**X**
ERA Chirp [14]		**X**			**X**	**X**
VF [26], [27], [28]		**X**		**X**	**X**	**X**
LBFI [16], [17], [18]		**X**			**X**	**X**
Proposed **QBBT**		**X**	**X**		**X**	**X**

monitoring of the frequency in a range of interest within the interpolation process.
- The proposed QBBT reduces the error associated with the identification of linear models concerning the LBFI technique applied in power systems in [17] (LBFI also uses frequency data), achieving a small absolute error in the magnitude of the frequency response of the models of the order of 1.00×10^{-3} dB.
- The new QBBT formulation makes use of the SVD, thereby the obtained models, besides accuracy, have a reduced number of state variables which manage to describe the power system linear behavior.

II. Mathematical Fundamentals

Let's consider a power system model as an LTI dynamical system in descriptor form, represented by

$$\begin{aligned} \mathbf{E}\dot{\mathbf{x}}(t) &= \mathbf{A}\mathbf{x}(t) + \mathbf{B}\mathbf{u}(t), \mathbf{x}(0) = \mathbf{x}_0, \\ \mathbf{y}(t) &= \mathbf{C}\mathbf{x}(t) + \mathbf{D}\mathbf{u}(t) \end{aligned} \tag{1}$$

where $\mathbf{E} \in \mathbb{R}^{n,n}$, $\mathbf{A} \in \mathbb{R}^{n,n}$, $\mathbf{B} \in \mathbb{R}^{n,m}$, $\mathbf{C} \in \mathbb{R}^{p,n}$, and $\mathbf{D} \in \mathbb{R}^{p,m}$ are the model's forming matrices, $\mathbf{x}(t) \in \mathbb{R}^n$ is the vector of states with full order n, and $\mathbf{u}(t) \in \mathbb{R}^m$ represents the control inputs and $\mathbf{y}(t) \in \mathbb{R}^p$ defines the system outputs from a MIMO system with p outputs and m inputs, respectively. The initial condition of the states is known and represented by $\mathbf{x}_0 \in \mathbb{R}^n$. Under this form, the transfer function of (1) can be expressed as:

$$\mathbf{H}(s) = \mathbf{C}(s\mathbf{E} - \mathbf{A})^{-1}\mathbf{B} + \mathbf{D} \tag{2}$$

A. Balanced Truncation

From the classical formulation of BT, the controllability and observability Gramians are calculated from (1), by using the Lyapunov equations [8], such that:

$$\begin{aligned} \mathbf{A}\mathbf{P}\mathbf{E}^T + \mathbf{E}\mathbf{P}\mathbf{A}^T + \mathbf{B}\mathbf{B}^T &= 0 \\ \mathbf{A}^T\mathbf{Q}\mathbf{E} + \mathbf{E}^T\mathbf{Q}\mathbf{A} + \mathbf{C}^T\mathbf{C} &= 0 \end{aligned} \tag{3}$$

where $\mathbf{P}$ and $\mathbf{Q}$ are respectively the controllability and observability Gramians, and they are defined in the frequency domain as [8]:

$$\mathbf{P} = \frac{1}{2\pi}\int_{-\infty}^{\infty} (i\varsigma\mathbf{E} - \mathbf{A})^{-1}\mathbf{B}\mathbf{B}^{-1}(-i\varsigma\mathbf{E}^T - \mathbf{A}^T)^{-1}d\varsigma \tag{4}$$

$$\mathbf{Q} = \frac{1}{2\pi}\int_{-\infty}^{\infty} \left(-i\omega\mathbf{E}^T - \mathbf{A}^T\right)^{-1}\mathbf{C}^{-1}\mathbf{C}(i\omega\mathbf{E} - \mathbf{A})^{-1}d\omega \tag{5}$$

To calculate $\mathbf{P}$ and $\mathbf{Q}$ via BT, the Lyapunov equations in (3) are solved requiring access to the linear model, which makes BT a ROM method but not a data-driven identification technique. Then, a balanced realization of the reduced order system can be derived in the form [8]:

$$\begin{aligned} \mathbf{E}_r\dot{\mathbf{x}}_r(t) &= \mathbf{A}_r\mathbf{x}_r(t) + \mathbf{B}_r\mathbf{u}(t), \mathbf{x}_r(0) = \mathbf{x}_0, \\ \mathbf{y}_r(t) &= \mathbf{C}_r\mathbf{x}_r(t) + \mathbf{D}_r\mathbf{u}(t) \end{aligned} \tag{6}$$

where $\mathbf{x}_r(t) \in \mathbb{R}^r$ is the reduced vector of state with order r.

B. Quadrature-based Balanced Truncation

Contrary to the BT statements, the QBBT proposes expressing the Gramians (4) and (5) through approximations formed by a sum of terms. Thus, a quadrature rule is advocated for the selection of these terms associated with weight vectors, thereby the approximated Gramians become [25]:

$$\begin{aligned} \tilde{\mathbf{P}} = \textstyle\sum_{j=1}^{N_p} \rho_j^2 (i\varsigma_j\mathbf{E} - \mathbf{A})^{-1}\mathbf{B}\mathbf{B}^T(-i\varsigma_j\mathbf{E}^T - \mathbf{A}^T)^{-1} + \\ + \rho_\infty^2\mathbf{E}^{-1}\mathbf{B}\mathbf{B}^T\mathbf{E}^{-T} \end{aligned} \tag{7}$$

$$\begin{aligned} \tilde{\mathbf{Q}} = \textstyle\sum_{k=1}^{N_q} \phi_k^2 \left(-i\omega_k\mathbf{E}^T - \mathbf{A}^T\right)^{-1}\mathbf{C}^T\mathbf{C}(i\omega_k\mathbf{E} - \mathbf{A})^{-1} + \\ + \phi_\infty^2\mathbf{E}^{-T}\mathbf{C}^T\mathbf{C}\mathbf{E}^{-1} \end{aligned} \tag{8}$$

where ρ_j and ϕ_k are the weights associated with the frequency points $i\varsigma_j$ and $i\omega_k$, respectively; and N_p and N_q are the number of frequency points used. Under these approximations, the weights ρ_∞ and ϕ_∞ are associated with points at infinity according to the selected quadrature rule. In this way, a numerical solution to (4) and (5), in an implicit manner, can be derived by employing a quadrature rule for the selection of frequency points and the calculation of their associated weights. Thus, a QBBT-based balanced realization of the system, based on the Gramians' approximations, is achieved in the form [25]:

$$\begin{aligned} \tilde{\mathbf{E}}_r\dot{\tilde{\mathbf{x}}}_r(t) &= \tilde{\mathbf{A}}_r\tilde{\mathbf{x}}_r(t) + \tilde{\mathbf{B}}_r\mathbf{u}(t), \tilde{\mathbf{x}}_r(0) = \mathbf{x}_0, \\ \tilde{\mathbf{y}}_r(t) &= \tilde{\mathbf{C}}_r\tilde{\mathbf{x}}_r(t) + \tilde{\mathbf{D}}_r\mathbf{u}(t) \end{aligned} \tag{9}$$

where r corresponds to the new order of this representation, and matrices $\tilde{\mathbf{E}}_r \in \mathbb{R}^{r,r}$, $\tilde{\mathbf{A}}_r \in \mathbb{R}^{r,r}$, $\tilde{\mathbf{B}}_r \in \mathbb{R}^{r,m}$, $\tilde{\mathbf{C}}_r \in \mathbb{R}^{p,r}$, and $\tilde{\mathbf{D}}_r \in \mathbb{R}^{p,m}$ can be obtained via the QBBT method using the set of real value matrices $\tilde{\mathbb{L}}_{\mathrm{R}}$, $\tilde{\mathbb{M}}_{\mathrm{R}}$, $\tilde{\mathbb{H}}_{\mathrm{R}}$ and $\tilde{\mathbb{G}}_{\mathrm{R}}$ [25]. These matrices are obtained from the interpolation of the $i\varsigma_j$ and $i\omega_k$ frequency points, the ρ_j and ϕ_k weights, and the $\mathbf{H}(i\varsigma_j)$ and $\mathbf{H}(i\omega_k)$ frequency maps, extracted from a dynamic system dataset. It is important to note that although matrices $\mathbf{E}$, $\mathbf{A}$, $\mathbf{B}$, $\mathbf{C}$ and $\mathbf{D}$ appear in (7) and (8), the application of the QBBT method does not require knowledge of them, as can be seen in the stages for its application.

C. Adjustments of Quadrature Rules

Quadrature rules provide numerical solutions to different mathematical operations such as integration. For instance, the authors in [35] use different mapping functions to obtain numerical approximations of indefinite integrals in different coordinate systems; meanwhile, the quadrature rule proposed in [36] approximate solutions to semi-definite integrals using Chebyshev polynomials.

In this work, the terms of the Gramians' approximations shown in (7) and (8) are selected from the BCC quadrature rule [37]. In [25], the authors worked from this rule for the QBBT's application based on dynamics characterized by their transfer functions. In this paper, an adjustment of the quadrature rule is needed for its application to power systems.

D. Boyd/Clenshaw-Curtis quadrature rule

The Boyd/Clenshaw-Curtis quadrature rule in [37] solves indefinite integrals by approximations. For instance, let $\mathbf{F}(\vartheta)$

be an integrable function in $[-\infty, \infty]$, which can be mapped into a new space such that $\vartheta = L\ cot\,(\tau)$, $\forall \tau \in [0, \pi]$, then the integral of $\mathbf{F}(\vartheta)$ becomes [37]:

$$\int_{-\infty}^{\infty} \mathbf{F}\,(\vartheta)\,d\vartheta = \int_{0}^{\pi} \frac{\mathbf{F}\,(L\cot\,(\tau))\,L}{\sin^2\,(\tau)} d\tau \tag{10}$$

where L is a truncation constant in the domain of the mapping function that must be adjusted, bounding the integration into a certain interval within the domain of the original function. In this way, the integration in the domain of the mapping function $[0, \pi]$ can be solved by selecting a certain number of quadrature points within the interval. If the points are selected equidistantly, the distance (h) among them can be calculated as:

$$h = \frac{\pi}{N+1}, N \in \mathbb{N} \tag{11}$$

where N is the number of quadrature points. The value of the ℓ-th quadrature point (τ_ℓ) in the interval $[0, \pi]$ is expressed as:

$$\tau_\ell = \ell h,\ \ell = 1, 2, 3, ..., N \tag{12}$$

Finally, the integral in (10) can be approximated as a sum of N terms, resulting in:

$$\int_{-\infty}^{\infty} \mathbf{F}\,(\vartheta)\,d\vartheta \approx \sum_{\ell=1}^{N} hL \frac{\mathbf{F}\,(L\cot\,(\tau_\ell))}{\sin^2\,(\tau_\ell)} + \frac{h}{L}\mathbf{M} \tag{13}$$

The number of terms and the truncation constant are adjustment parameters of the BCC rule. Under this quadrature rule, there exists a point at infinity ($\frac{h}{L}\mathbf{M}$), where $\mathbf{M}$ is a Markov parameter that corresponds to the vertical asymptote of the mapping function at $\tau = 0$ and $\tau = \pi$. When this quadrature rule uses the weights associated with each one of the points, the approximation is expressed as [25], [37]:

$$\int_{-\infty}^{\infty} \mathbf{F}\,(\vartheta)\,d\vartheta \approx \sum_{\ell=1}^{N} \gamma_\ell^2 \mathbf{F}\,(\tau_\ell) \tag{14}$$

where the frequency points ϑ_ℓ and the weights γ_ℓ can be obtained by

$$\vartheta_\ell = L\cot\,(\tau_\ell) \tag{15}$$

$$\gamma_\ell = \sqrt{\frac{L\pi}{(N+1)\sin^2\,\tau_\ell}} \tag{16}$$

By applying this quadrature rule to the approximation of the Gramians $\mathbf{P}$ and $\mathbf{Q}$ in (7) and (8), respectively, the quadrature points τ_j, frequency points $\hat{\varsigma}_j$, and weights $\hat{\rho}_j$ associated with the approximation $\tilde{\mathbf{P}}$ based on the selection of N_p points in quadrature and the adjustment of the truncation constant L_p. Similarly, τ_k, $\hat{\omega}_k$, and $\hat{\phi}_k$ are associated with the approximation $\tilde{\mathbf{Q}}$ from the selection of N_q points in quadrature and the adjustment of L_q. For the application of QBBT, $N_p = N_q$ and $L_p < L_q$ will be adjusted to achieve rational interpolation.

The quadrature points τ_j and τ_k are calculated using (12). It has the same value in positions $j = k$ as a result of the adjustment $N_p = N_q$. From these quadrature points and using the truncation constants L_p and L_q, their weights $\hat{\rho}_j$ and $\hat{\phi}_k$ are calculated using (16). The frequency points $i\hat{\varsigma}_j$ and $i\hat{\omega}_k$, derived from the quadrature points, are obtained by (15). The distribution of these frequency points is shown in Fig. 1.

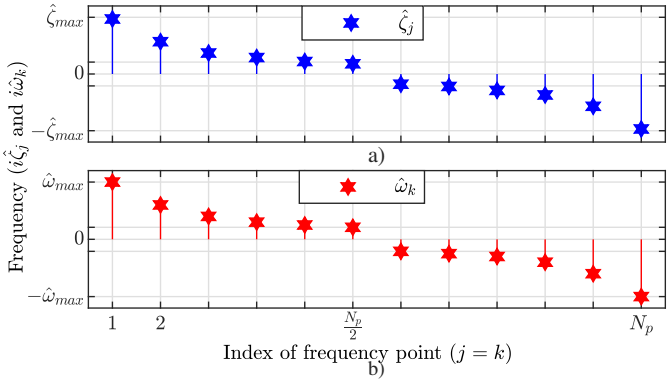

Fig. 1. Unsorted frequency points: a) frequency points for $\tilde{\mathbf{P}}$ approximation; and b) frequency points for $\tilde{\mathbf{Q}}$ approximation.

As seen in Fig. 1, the distribution of these points is associated with the decreasing monotony of the mapping function. By selecting the same number of points for both approaches and $L_p < L_q$, the highest frequency value for which the model to be identified will be valid is found in the first position of the frequency vector $i\hat{\omega}_k$. This value can be calculated by substituting (11) and (12) into (15), for $k = 1$ as:

$$\hat{\omega}_{max} = L_q \cot(\frac{\pi}{N_q + 1}) \tag{17}$$

The maximum frequency calculated by (17) corresponds to the highest frequency at which the model will be valid and can be expressed in [Hz] as $f_{max} = \frac{\hat{\omega}_{max}}{2\pi}$. This frequency range is directly related to the selection of truncation constants and the number of quadrature points for each approximation. The selection of different values of L_p and L_q ensures that $\hat{\varsigma}_j$ and $\hat{\omega}_k$ are disjoint.

E. Sorting of Frequency Points and Weights

The QBBT method employs rational interpolation, which requires a data sorting stage. The process of sorting the frequency points and their respective weights is carried out as

$$j \leq \frac{N_p}{2} \begin{cases} \varsigma_{N_p - 2j+1} = \hat{\varsigma}_j \\ \rho_{N_p - 2j+1} = \hat{\rho}_j \end{cases} \quad j > \frac{N_p}{2} \begin{cases} \varsigma_{2j - N_p} = \hat{\varsigma}_j \\ \rho_{2j - N_p} = \hat{\rho}_j \end{cases} \tag{18}$$

$$k \leq \frac{N_q}{2} \begin{cases} \omega_{N_q - 2k+1} = \hat{\omega}_k \\ \phi_{N_q - 2k+1} = \hat{\phi}_k \end{cases} \quad k > \frac{N_q}{2} \begin{cases} \omega_{2k - N_q} = \hat{\omega}_k \\ \phi_{2k - N_q} = \hat{\phi}_k \end{cases} \tag{19}$$

where $j = 1, 2, 3, ..., N_p$ and $k = 1, 2, 3, ..., N_q$.

Starting from (18) and (19) in the odd positions of the vectors ς_j and ω_k, the positive frequencies are positioned in ascending order until they cover the entire frequency range under study; and consecutively in the even positions their respective negative values. Likewise, the weights are associated with their respective frequencies, they are ordered in the same way, such that these relationships are retained.

F. Frequency Maps Extraction

For the application of QBBT, the frequency maps $\mathbf{H}(i\varsigma_j)$ and $\mathbf{H}(i\omega_k)$ are extracted from the system under study at the frequency points. The frequency points $i\varsigma_j$ and their weights

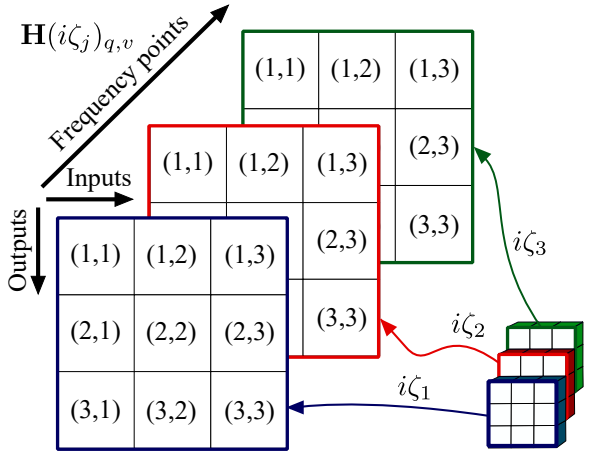

Fig. 2. Frequency maps $\mathbf{H}(i\varsigma_j)$ in tensor form.

ρ_j are associated with the approximation $\tilde{\mathbf{P}}$, and the frequency points $i\omega_k$ and their weights ϕ_k are associated with the approximation $\tilde{\mathbf{Q}}$.

Frequency maps are arrays of matrices or tensors, which contain the behavior of all the outputs of the system concerning all its inputs for a certain range of frequencies. Fig. 2 shows this structure for a system of $q = 1, 2, 3$ outputs, $v = 1, 2, 3$ inputs, and $j = 1, 2, 3$ frequency points in the vector $i\varsigma_j$.

As can be seen in Fig. 2, the rows of each matrix correspond to the outputs of the system and the columns to the inputs, forming a matrix for each frequency point. In each element of the matrices, the output/input relationships are stored for a frequency range and represented by $\mathbf{H}(i\varsigma_j)_{q,v}$, which correspond to the transfer function of a system in (1), which can also be expressed as:

$$\mathbf{H}(i\varsigma_j)_{q,v} = \frac{\mathbf{Y}(i\varsigma_j)_{q,v}}{\mathbf{U}(i\varsigma_j)_v} \tag{20}$$

where $\mathbf{H} \in \mathbb{C}^{p,v,j}$, $\mathbf{Y} \in \mathbb{C}^{p,v,j}$ and $\mathbf{U} \in \mathbb{C}^{v,j}$ respectively represent the frequency output and input datasets, such that $q = 1, 2, 3, ..., p$, $v = 1, 2, 3, ..., m$ and $j = 1, 2, 3, ..., N_p$; p is the number of outputs, m is the number of inputs, and N_p is the number of frequency points selected in the $\tilde{\mathbf{P}}$ approximation. In the $\tilde{\mathbf{Q}}$ approximation, this representation is valid for the frequency map in $\mathbf{H}(i\omega_k)_{q,v}$, where the difference lies in the use of the N_q frequency points into $i\omega_k$.

G. Interpolation Matrices Calculation

Since the frequency points and their associated weights are available along with the frequency maps, then the following definitions can be applied to carry out rational interpolation [25]:

$$\tilde{\mathbb{L}}_{k,j} = \begin{bmatrix} \phi_1\rho_1 \frac{\mathbf{H}(i\omega_1)-\mathbf{H}(i\varsigma_1)}{i\omega_1 - i\varsigma_1} & \cdots & \phi_1\rho_j \frac{\mathbf{H}(i\omega_1)-\mathbf{H}(i\varsigma_j)}{i\omega_1 - i\varsigma_j} \\ \vdots & \ddots & \vdots \\ \phi_k\rho_1 \frac{\mathbf{H}(i\omega_k)-\mathbf{H}(i\varsigma_1)}{i\omega_k - i\varsigma_1} & \cdots & \phi_k\rho_j \frac{\mathbf{H}(i\omega_k)-\mathbf{H}(i\varsigma_j)}{i\omega_k - i\varsigma_j} \end{bmatrix} \tag{21}$$

$$\tilde{\mathbb{M}}_{k,j} = \begin{bmatrix} \phi_1\rho_1 \frac{i\omega_1\mathbf{H}(i\omega_1)-i\varsigma_1\mathbf{H}(i\varsigma_1)}{i\omega_1 - i\varsigma_1} & \cdots & \phi_1\rho_j \frac{i\omega_1\mathbf{H}(i\omega_1)-i\varsigma_j\mathbf{H}(i\varsigma_j)}{i\omega_1 - i\varsigma_j} \\ \vdots & \ddots & \vdots \\ \phi_k\rho_1 \frac{i\omega_k\mathbf{H}(i\omega_k)-i\varsigma_1\mathbf{H}(i\varsigma_1)}{i\omega_k - i\varsigma_1} & \cdots & \phi_k\rho_j \frac{i\omega_k\mathbf{H}(i\omega_k)-i\varsigma_j\mathbf{H}(i\varsigma_j)}{i\omega_k - i\varsigma_j} \end{bmatrix} \tag{22}$$

$$\tilde{\mathbb{H}}_k = \begin{bmatrix} \phi_1\mathbf{H}(i\omega_1)]^T & \phi_2\mathbf{H}(i\omega_2)^T & \dots & \phi_k\mathbf{H}(i\omega_k)^T \end{bmatrix}^T \tag{23}$$

$$\tilde{\mathbb{G}}_j = \begin{bmatrix} \rho_1\mathbf{H}(i\varsigma_1) & \rho_2\mathbf{H}(i\varsigma_2) & \dots & \rho_j\mathbf{H}(i\varsigma_j) \end{bmatrix} \tag{24}$$

where $\tilde{\mathbb{L}} \in \mathbb{C}^{pN_p \times N_p m}$, $\tilde{\mathbb{M}} \in \mathbb{C}^{pN_p \times N_p m}$, $\tilde{\mathbb{H}} \in \mathbb{C}^{pN_p \times m}$ and $\tilde{\mathbb{G}} \in \mathbb{C}^{p \times N_p m}$ are matrices for a MIMO system with p outputs and m inputs.

H. Linear Model Identification

It is desired to identify a real model, so the previously calculated matrices must be transformed into real equivalents. For this purpose, a change of base is made, and the new real matrices are calculated by

$$\begin{aligned} \tilde{\mathbb{L}}_{\mathrm{R}} &= \mathbf{G}_l^* \tilde{\mathbb{L}} \mathbf{G}_r, \tilde{\mathbb{M}}_{\mathrm{R}} = \mathbf{G}_l^* \tilde{\mathbb{M}} \mathbf{G}_r \\ \tilde{\mathbb{H}}_{\mathrm{R}} &= \mathbf{G}_l^* \tilde{\mathbb{H}}, \quad \tilde{\mathbb{G}}_{\mathrm{R}} = \tilde{\mathbb{G}} \mathbf{G}_r \end{aligned} \tag{25}$$

where $\mathbf{G}_l$ and $\mathbf{G}_r$ are obtained by diagonalizing $\frac{N_p}{2}$ times to I_l and $\frac{N_q}{2}$ times to I_r, respectively. I_l and I_r are calculated as:

$$\mathbf{I}_l = \frac{1}{\sqrt{2}} \begin{bmatrix} \mathbf{I}_p & -i\mathbf{I}_p \\ \mathbf{I}_p & +i\mathbf{I}_p \end{bmatrix}, \mathbf{I}_r = \frac{1}{\sqrt{2}} \begin{bmatrix} \mathbf{I}_m & -i\mathbf{I}_m \\ \mathbf{I}_m & +i\mathbf{I}_m \end{bmatrix} \tag{26}$$

where $I_p \in \mathbb{R}^{p \times p}$ and $I_m \in \mathbb{R}^{m \times m}$ are identity matrices, whose dimensions are associated with the number of outputs and inputs.

Once all matrices have been converted to their real equivalents, the SVD $\tilde{\mathbb{L}}_{\mathrm{R}} = \tilde{\mathbf{Z}}\tilde{\mathbf{S}}\tilde{\mathbf{Y}}$ is performed. More precisely the SVD is expressed as [22], [38]:

$$\tilde{\mathbb{L}}_{\mathrm{R}} = \begin{bmatrix} \tilde{\mathbf{Z}}_1 & \tilde{\mathbf{Z}}_2 \end{bmatrix} \begin{bmatrix} \tilde{\mathbf{S}}_1 & \\ & \tilde{\mathbf{S}}_2 \end{bmatrix} \begin{bmatrix} \tilde{\mathbf{Y}}_1^* \\ \tilde{\mathbf{Y}}_2^* \end{bmatrix} \tag{27}$$

The singular values are arranged in descending order on the main diagonal of the matrix $\tilde{\mathbf{S}}$ decomposed into the matrices $\tilde{\mathbf{S}}_1$ and $\tilde{\mathbf{S}}_2$ as follows:

$$\begin{bmatrix} \tilde{\mathbf{S}}_1 & \\ & \tilde{\mathbf{S}}_2 \end{bmatrix} = \begin{bmatrix} \sigma_1 & 0 & 0 & 0 & 0 & 0 & 0 \\ 0 & \sigma_2 & 0 & 0 & 0 & 0 & 0 \\ 0 & 0 & \ddots & 0 & 0 & 0 & 0 \\ 0 & 0 & 0 & \sigma_r & 0 & 0 & 0 \\ 0 & 0 & 0 & 0 & \sigma_{r+1} & 0 & 0 \\ 0 & 0 & 0 & 0 & 0 & \ddots & 0 \\ 0 & 0 & 0 & 0 & 0 & 0 & \sigma_n \end{bmatrix} \tag{28}$$

where $\tilde{\mathbf{S}}_1 \in \mathbb{R}^{r \times r}$ is obtained by selecting the order r of the system to be identified. In the same way, $\tilde{\mathbf{Z}}_1$ is obtained by truncating their first r columns of $\tilde{\mathbf{Z}}$ and $\tilde{\mathbf{Y}}_1$ by truncating their first r rows of $\tilde{\mathbf{Y}}$. Matrices $\tilde{\mathbf{Z}}_1$, $\tilde{\mathbf{S}}_1$ and $\tilde{\mathbf{Y}}_1$ are only used for the identification, thus the uncontrollable and unobservable states of the system are neglected. The new model S_r of the system via the QBBT method can be calculated using the definition [25]:

$$\tilde{S}_r \begin{cases} \tilde{\mathbf{E}}_r &= -\tilde{\mathbf{S}}_1^{-1/2} \tilde{\mathbf{Z}}_1^* \tilde{\mathbb{L}}_{\mathrm{R}} \tilde{\mathbf{Y}}_1 \tilde{\mathbf{S}}_1^{-1/2} \\ \tilde{\mathbf{A}}_r &= -\tilde{\mathbf{S}}_1^{-1/2} \tilde{\mathbf{Z}}_1^* \tilde{\mathbb{M}}_{\mathrm{R}} \tilde{\mathbf{Y}}_1 \tilde{\mathbf{S}}_1^{-1/2} \\ \tilde{\mathbf{B}}_r &= \tilde{\mathbf{S}}_1^{-1/2} \tilde{\mathbf{Z}}_1^* \tilde{\mathbb{H}}_{\mathrm{R}} \\ \tilde{\mathbf{C}}_r &= \tilde{\mathbb{G}}_{\mathrm{R}}^T \tilde{\mathbf{Y}}_1 \tilde{\mathbf{S}}_1^{-1/2} \\ \tilde{\mathbf{D}}_r &= 0 \end{cases} \tag{29}$$

Algorithm 1 Boyd/Clenshaw-Curtis quadrature rule.

1: **Input:** N_p, N_q, L_p and L_q
2: **Ensure:** $N_p = N_q$, $L_p < L_q$
3: **Output:** $[\hat{\varsigma}_j, \hat{\omega}_k, \hat{\rho}_j, \hat{\phi}_k]$
4: $h \leftarrow N_p$;
5: $\tau_j \leftarrow h, j = 1, 2, ..., N_p$ and $\tau_k \leftarrow h, k = 1, 2, ..., N_q$;
6: $\hat{\varsigma}_j \leftarrow [L_p, \tau_j]$ and $\hat{\omega}_k \leftarrow [L_q, \tau_k]$;
7: $\hat{\rho}_j \leftarrow [L_p, N_p, \tau_j]$ and $\hat{\phi}_k \leftarrow [L_q, N_q, \tau_k]$;
8: **return** $[\hat{\varsigma}_j, \hat{\omega}_k, \hat{\rho}_j, \hat{\phi}_k]$

In this context, a new approach was given to the BT technique under its classical formulation, combining the use of the BCC quadrature rule for the selection of frequency points and the calculation of their associated weights, and obtaining a linear model through rational interpolation.

III. Quadrature-Based Balanced Truncation on Power System

To incorporate QBBT into power systems, a frequency range in which the identified model is valid must be defined. The range will be selected ensuring the inclusion of inter-area oscillation modes $[0.1 : 0.8]$ Hz and local oscillation modes $[0.8 : 2]$ Hz, defined in [39]. This can be possible through an adequate quadrature rule adjustment.

Based on the BCC quadrature rule, frequency points, and associated weights will be obtained. The frequency maps of the power system will be extracted through transient simulations and the fast Fourier transform (FFT). Finally, QBBT definitions will be applied.

A. Boyd/Clenshaw-Curtis Quadrature Rule Adjustment

To select the required frequency points and calculate their associated weights via the BCC quadrature rule, it is necessary to adjust the parameters N_p, N_q, L_p, and L_q. Then, the frequency points $\hat{\varsigma}_j$ and $\hat{\omega}_k$ and the weights $\hat{\rho}_j$ and $\hat{\phi}_k$, are calculated using **Algorithm 1**.

The calculation of the frequency points and their associated weights comprise the first stage of the identification process exhibited in Fig. 3. In this stage, the frequency range is defined from the maximum frequency point contained in $\hat{\omega}_k$ and calculated using (17).

B. Frequency Points and Weights Sorting

To guarantee the rational interpolation of the frequency data associated with the Gramians' approximations, these must be sorted in the way shown in (18) and (19). The sorting process is carried out through **Algorithm 2**.

When sorting the frequency points, their associated weights are sorted in the same way to retain the original relationship.

C. Frequency maps Extraction

To extract the frequency maps from power systems, the Power System Toolbox (PST) is used [40]. Considering the system as a black-box model, as shown in Fig. 3, in which there is only access to a group of inputs and outputs. The reference voltages of the excitation systems $Vref$ of all the generators are considered as inputs, and the set of the angular velocity of the rotors ωg of all generators and the voltage magnitude $|V|$ of all buses of the system are considered as outputs. Power systems with ng generators and nb buses are represented as a MIMO system with $q = 1, 2, 3, ..., m$ inputs, $v = 1, 2, 3, ..., p$ outputs, where $m = ng$ and $p = ng + nb$.

Once the frequency points ς_j and ω_k are calculated and sorted using **Algorithm 1** and **Algorithm 2**, transient simulations are performed using the PST function ***s_simu.m***. Through the PST function ***mexc_sig.m***, each input is individually modulated using the signal models $\mathbf{u}_v = \alpha \sin(\varsigma_j t + \varphi_0)$ and $\mathbf{u}_v = \alpha \sin(\omega_k t + \varphi_0)$ for each frequency point ς_j and ω_k, respectively; where α is the magnitude of these signals and φ_0 is the phase. In this modulation process, $\alpha = 0.001$

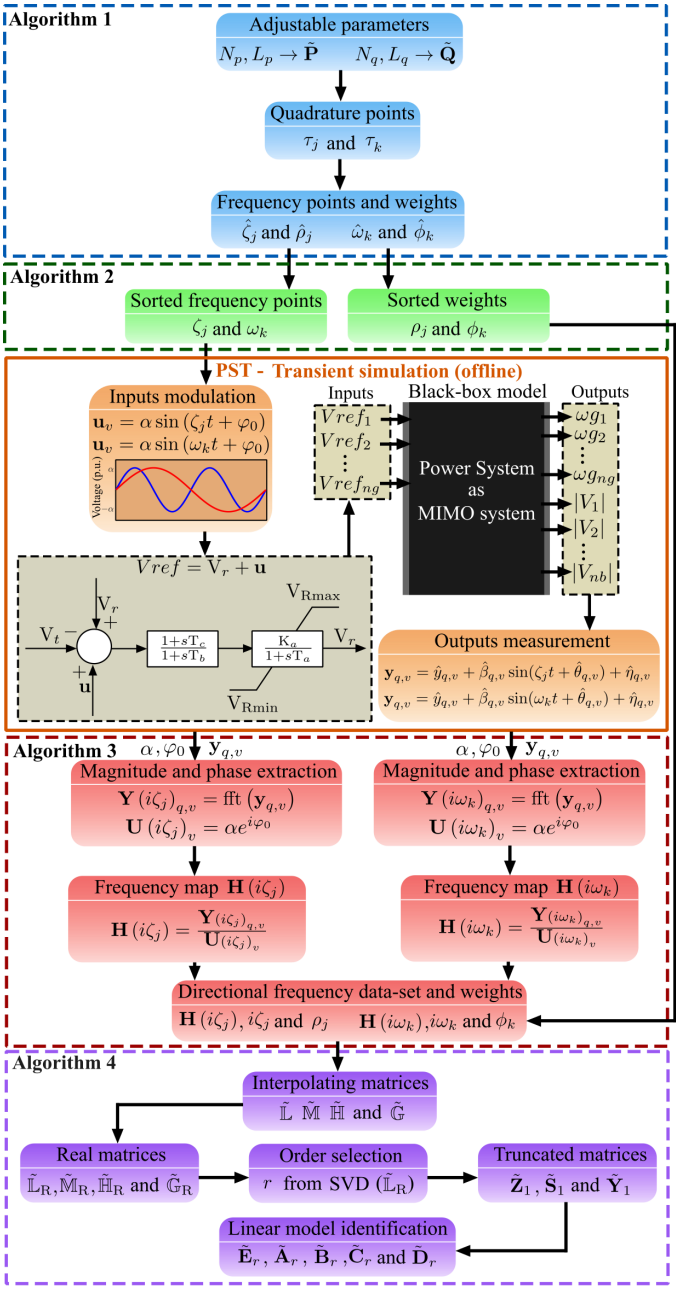

Fig. 3. Flowchart for the QBBT application in power systems.

Algorithm 2 Sorting of frequency points and weights.

Input: $\hat{\varsigma}_j$, $\hat{\omega}_k$, $\hat{\rho}_j$ and $\hat{\phi_k}$
Output: $[\varsigma_j, \omega_k, \rho_j, \phi_k]$
for $j = 1\ to\ N_p$ **do**
  if $j \leq \frac{N_p}{2}$ **then**
    $\varsigma_{N_p-2j+1} \leftarrow \hat{\varsigma}_j$ and $\rho_{N_p-2j+1} \leftarrow \hat{\rho}_j$;
  else
    $\varsigma_{2j-N_p} \leftarrow \hat{\varsigma}_j$ and $\rho_{2j-N_p} \leftarrow \hat{\rho}_j$;
  end if
end for
for $k = 1\ to\ N_q$ **do**
  if $k \leq \frac{N_p}{2}$ **then**
    $\omega_{N_q-2k+1} \leftarrow \hat{\omega}_k$ and $\phi_{N_q-2k+1} \leftarrow \hat{\phi}_k$;
  else
    $\omega_{2k-N_q} \leftarrow \hat{\omega}_k$ and $\phi_{2k-N_q} \leftarrow \hat{\phi}_k$;
  end if
end for
return $[\varsigma_j, \omega_k, \rho_j, \phi_k]$

Algorithm 3 Frequency maps extraction.

Input: $\mathbf{y}_{q,v}$, α, φ_0, ς_j, N_p, p and m
Output: $[i\varsigma_j, \mathbf{H}(i\varsigma_j)]$
for $j = 1\ to\ N_p$ **do**
  if j is odd **then**
    for $v = 1\ to\ m$ **do**
      for $q = 1\ to\ p$ **do**
        $(\beta_{q,v}, \theta_{q,v})$; $\leftarrow$fft$(\mathbf{y}_{q,v})$
      end for
    end for
    $Re\{[\mathbf{H}(i\varsigma_j)]_{q,p}\} \leftarrow Re\left\{\frac{\beta_{q,p}}{\alpha} e^{i(\theta_{q,p}-\varphi_0)}\right\}$;
    $Im\{[\mathbf{H}(i\varsigma_j)]_{q,p}\} \leftarrow Im\left\{\frac{\beta_{q,p}}{\alpha} e^{i(\theta_{q,p}-\varphi_0)}\right\}$;
  else
    $Re\{[\mathbf{H}(i\varsigma_j)]_{q,p}\} \leftarrow Re\{[\mathbf{H}(i\varsigma_{j-1})]_{q,p}\}$;
    $-Im\{[\mathbf{H}(i\varsigma_j)]_{q,p}\} \leftarrow Im\{[\mathbf{H}(i\varsigma_{j-1})]_{q,p}\}$;
  end if
end for
return $[i\varsigma_j, \mathbf{H}(i\varsigma_j)]$

is used to prevent the stimulations of nonlinearities, and φ_0 is assumed zero.

By modulating the system inputs, a sinusoidal behavior is expected at the outputs of the form $\mathbf{y}_{q,v} = \hat{y}_{q,v} + \hat{\beta}_{q,v} \sin\left(\varsigma_j t + \hat{\theta}_{q,v}\right) + \hat{\eta}_{q,v}$ and $\mathbf{y}_{q,v} = \hat{y}_{q,v} + \hat{\beta}_{q,v} \sin\left(\omega_k t + \hat{\theta}_{q,v}\right) + \hat{\eta}_{q,v}$, for the frequency points ς_j and ω_k, respectively; where $\hat{y}_{q,v}$ and $\hat{\eta}_{q,v}$ are offset values, which are removed using the Matlab function ***movmean.m***; $\hat{\beta}_{q,v}$ and $\hat{\theta}_{q,v}$ are the magnitude and angle of the output signals that are extracted using the FFT.

Then, the frequency maps $\mathbf{H}(i\varsigma_j)$ and $\mathbf{H}(i\omega_k)$, in the form presented in (20) and according to the structure shown in Fig. 2, can be constructed from the magnitudes and angles of the power system outputs/inputs relationship. **Algorithm 3** is used to extract the frequency map $\mathbf{H}(i\varsigma_j)$ from the frequency points ς_j in the input signals, and it is also used to obtain the frequency map $\mathbf{H}(i\omega_k)$ from the frequency points $i\omega_k$ as shown in the red section of Fig. 3.

D. Quadrature-Based Balanced Truncation Application

To identify a linear model of the system using the QBBT method, it is necessary to calculate the interpolation matrices $\tilde{\mathbb{L}}$, $\tilde{\mathbb{M}}$, $\tilde{\mathbb{H}}$ and $\tilde{\mathbb{G}}$ from the datasets $[i\varsigma_j, \mathbf{H}(i\varsigma_j), \rho_j]$ and $[i\omega_k, \mathbf{H}(i\omega_k), \phi_k]$ by using **Algorithm 4**.

These matrices are converted to real matrices to find a real power system linear model. Subsequently, the SVD of $\tilde{\mathbb{L}}_{\mathrm{R}}$ is

Algorithm 4 Quadrature-Based Balanced Truncation.

Input: $i\varsigma_j, i\omega_k, \rho_j, \phi_k, \mathbf{H}(i\varsigma_j)$ and $\mathbf{H}(i\omega_k)$
Output: $[\tilde{\mathbf{E}}_r, \tilde{\mathbf{A}}_r, \tilde{\mathbf{B}}_r, \tilde{\mathbf{C}}_r, \tilde{\mathbf{D}}_r]$
$[\tilde{\mathbb{L}}, \tilde{\mathbb{M}}, \tilde{\mathbb{H}}, \tilde{\mathbb{G}}] \leftarrow [i\varsigma_j, i\omega_k, \rho_j, \phi_k, \mathbf{H}(i\varsigma_j), \mathbf{H}(i\omega_k)]$
$[\tilde{\mathbb{L}}_{\mathrm{R}}, \mathbb{M}_{\mathrm{R}}, \mathbb{H}_{\mathrm{R}}, \mathbb{G}_{\mathrm{R}},] \leftarrow [\tilde{\mathbb{L}}, \mathbb{M}, \mathbb{H}, \mathbb{G}]$
$\mathbf{Z}\tilde{\mathbf{S}}\mathbf{Y}^* \leftarrow \tilde{\mathbb{L}}_{\mathrm{R}}$
$r \leftarrow \tilde{\mathbf{S}}$
$\tilde{\mathbf{Z}}_1 \leftarrow [\tilde{\mathbf{Z}}, r]$; $\tilde{\mathbf{S}}_1 \leftarrow [\tilde{\mathbf{S}}, r]$; $\tilde{\mathbf{Y}}_1 \leftarrow [\tilde{\mathbf{Y}}, r]$;
$\tilde{\mathbf{E}}_r \leftarrow [\tilde{\mathbf{S}}_1, \tilde{\mathbf{Z}}_1, \tilde{\mathbb{L}}_{\mathrm{R}}\tilde{\mathbf{Y}}_1, \tilde{\mathbf{S}}_1]$
$\tilde{\mathbf{A}}_r \leftarrow [\tilde{\mathbf{S}}_1, \tilde{\mathbf{Z}}_1, \mathbb{M}_{\mathrm{R}}\tilde{\mathbf{Y}}_1, \tilde{\mathbf{S}}_1]$
$\tilde{\mathbf{B}}_r \leftarrow [\tilde{\mathbf{S}}_1, \tilde{\mathbf{Z}}_1, \tilde{\mathbb{H}}_{\mathrm{R}}]$
$\tilde{\mathbf{C}}_r \leftarrow [\mathbb{G}_{\mathrm{R}}, \tilde{\mathbf{Y}}_1, \tilde{\mathbf{S}}_1]$
$\tilde{\mathbf{D}}_r \leftarrow 0$
return $[\tilde{\mathbf{E}}_r, \tilde{\mathbf{A}}_r, \tilde{\mathbf{B}}_r, \tilde{\mathbf{C}}_r, \tilde{\mathbf{D}}_r]$

TABLE II
BCC ADJUSTMENT CASES

Case	Points	Trunc. const.		Frequency range
	$N_p = N_q$	L_p	L_q	[Hz]
a)	10	18.00	18.44	[0.4119 - 9.9951]
b)	20	8.00	8.47	[0.1073 - 9.9996]
c)	30	6.00	6.38	[0.0484 - 9.9853]
d)	40	4.00	4.82	[0.0244 - 9.9919]
e)	50	3.00	3.87	[0.0147 - 9.9862]
f)	60	3.00	3.23	[0.0123 - 9.9728]
g)	70	2.00	2.78	[0.0070 - 9.9929]
h)	80	2.00	2.43	[0.0062 - 9.9665]

performed and the new order of the system r is calculated by applying the energy criterion used in [13] as

$$E_z = \frac{\sum_{z=1}^{n} \sigma_z}{\sum diag(\tilde{\mathbf{S}})}, z = 1, 2, 3, ..., n \tag{30}$$

where E_z is the energy of the first z singular values σ_z. When E_z reaches an adjustable threshold E_{th}, then the new order is determined by $r = z$. The adjustable thresholds of $E_{th} = 98\%$ and $E_{th} = 99\%$ are analyzed in the system identification process. Subsequently, the linear model $\tilde{S}_r$ is calculated using (29).

IV. APPLICATIONS TO POWER SYSTEMS

The QBBT method is applied to the Klein-Rogers-Kundur (KRK) power system, the NETS-NYPS, and the North-Eastern Power Coordination Council (NPCC). The frequency range for the identification of these three systems is set to a maximum value of 10.0 Hz that contains the inter-area and local modes. The number of quadrature points for Gramian approximations will be increased from 10 to 80 for each initial analysis considering $N_p = N_q$. Then, L_q will be calculated to ensure the maximum frequency value of 10.0 Hz, using (17) for each N_q adjustment. The value L_p will be adjusted to the real value that precedes the adjustment of L_q to guarantee rational interpolation ensuring that $L_p < L_q$. The settings corresponding to each previous case mentioned and calculated according to **Algorithm 1** are shown in Table II, before the sorting of frequency points and weights using **Algorithm 2**.

In this way, the models are identified and analyzed for each BCC quadrature rule adjustment attending first to the absolute error of frequency response and then to their order. The most balanced linear representation identified via QBBT in terms of the equilibrium between error and order, then they are compared with linear models obtained via LBFI in the KRK power system, the NETS-NYPS, and the NPCC.

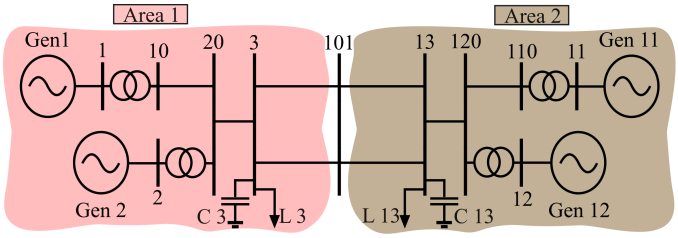

Fig. 4. Klein-Rogers-Kundur power system.

A. Klein-Rogers-Kundur Power System

As the first case study, the well-known KRK power system shown in Fig. 4, is selected. This test system has been used primarily for tuning power swing controllers. It is a small system that has two well-defined symmetrical areas and is made up of 13 buses, 4 generators, and 2 loads.

To identify the system, the frequency points $i\varsigma_j$ and $i\omega_k$ and the associated weights ρ_j and ϕ_k are calculated through the BCC quadrature rule settings presented in Table II, as well as the weights associated with these points ρ_j and ϕ_k. For each setting, datasets from the test systems are extracted from 200 s transient simulations using the Matlab environment-based PST. For this purpose, the function ***s_simu.m*** is used, which allows measuring the variables ωg and $|V|$ selected as outputs of the power system during the simulation. The transient simulations are carried out using the 4th-order transient model for generators equipped with static exciters modeled using a 1st-order model, representing a 5th-order model per generator and a 20th-order system for all generators in the KRK power system.

The excitation systems of all generators are modulated with the signal model mentioned in Section III-C. Two groups of simulations are thus carried out, one for the frequency points $i\varsigma_j$ and another for $i\omega_k$, to obtain the frequency maps $\mathbf{H}(i\varsigma_j)$ and $\mathbf{H}(i\omega_k)$ according to **Algorithm 3**. Once all the required data is available, the definitions shown in Section III-D are applied for $E_{th} = 98\%$ and $E_{th} = 99\%$ of the energy threshold in the SVD according to (30) and using **Algorithm 4**.

To validate the model identified by the QBBT method, we obtained an analytical model of the KRK power system using the PST function ***svm_mgen.m***, and the order of these linear representations is $n = 20$. Table III shows the largest absolute error of the frequency response for each setting of the BCC quadrature rule according to Table II, and for energy criteria $E_{th} = 98\%$ and $E_{th} = 99\%$.

As shown in Table III, the energy of the singular values in case a) for $E_{th} = 98\%$ and $E_{th} = 99\%$, only 10 quadrature points are used for each approximation and the largest error is obtained and the highest order in the models identified. The smaller errors are found in the models obtained for the energy criterion adjusted to 99% except for case a), and this error decreases to a constant value of 7.60×10^{-3} dB in case d) to h), also maintaining an order $r = 9$. Based on these results, the model obtained in case d) will be used for subsequent analysis for the energy adjustment of 99%, since only 40 quadrature points will be required for each approximation. The dimensions of the interpolation matrices calculated in this case and the matrices that make up the model are shown in Table IV.

TABLE III
KRK POWER SYSTEM LINEAR MODELS: ERROR AND ORDER

Case	a)	b)	c)	d)	e)	f)	g)	h)
Abs. Error $\times 10^{-2}$ (dB) E_{th}=98%	6.68	2.07	2.07	2.05	2.05	2.06	2.06	2.06
order (r)	9				7			
Abs. Error $\times 10^{-3}$ (dB) E_{th}=99%	32.20	9.60	9.60	7.60	7.60	7.60	7.60	7.60
order (r)	10	8	8			9		

As depicted in Table IV, the dimensions of the interpolating matrices calculated for the KRK power system are associated with 4 modulated inputs and 17 outputs measured during the identification process using the QBBT approach, as well as 40 quadrature points used in the approximation of each Gramian. Furthermore, the power system under study has a few well-known oscillatory modes, meaning that the identified linear model matrices are not of large dimensions. Fig. 5 shows the analysis of the frequency response of both models for a frequency range from 0 to 3.0 Hz.

As can be seen in Figure 5 a)-d), the model identified through QBBT manages to accurately preserve the frequency behavior of the system's analytical model and can capture the respective frequency at an inter-area mode of 0.613 Hz. In Figs. 5 a) and b), a frequency associated with a local oscillation mode of 1.164 Hz is captured, meanwhile in Figs. 5 c) and d) another local oscillation mode of 1.188 Hz appears.

For comparison purposes, the identification of the linear model of the KRK power system is carried out using the LBFI

TABLE IV
KRK POWER SYSTEM DIMENSION OF MATRICES FOR CASE d) AND $E_{th} = 99\%$

Interpolating matrices		**Model matrices**		
$\tilde{\mathbb{L}} \in \mathbb{C}^{680\times160}$	$\tilde{\mathbb{M}} \in \mathbb{C}^{680\times160}$	$\tilde{\mathbf{E}}_r \in \mathbb{R}^{9\times9}$	$\tilde{\mathbf{A}}_r \in \mathbb{R}^{9\times9}$	$\tilde{\mathbf{B}}_r \in \mathbb{R}^{9\times4}$
$\tilde{\mathbb{H}} \in \mathbb{C}^{680\times4}$	$\tilde{\mathbb{G}} \in \mathbb{C}^{17\times160}$	$\tilde{\mathbf{C}}_r \in \mathbb{R}^{17\times9}$	$\tilde{\mathbf{D}}_r \in \mathbb{R}^{17\times4}$	

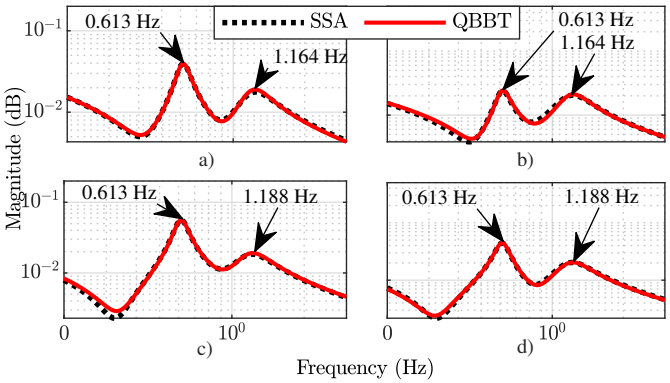

Fig. 5. Comparisons of frequency responses between SSA and QBBT for 4-outputs and 4-inputs in the KRK power system: a) output 1/input 1; b) output 2/input 2; c) output 3/input 3; d) output 4/input 4.

TABLE V
INTER-AREA OSCILLATING MODES OF THE KRK SYSTEM

SSA		BT		LBFI		QBBT	
Freq. (Hz)	D.r. (%)	Freq. (Hz)	D.r. (%)	Freq. (Hz)	D.r. (%)	Freq. (Hz)	D.r. (%)
± 1.178	18.659	±1.162	18.576	±1.155	19.217	±1.188	15.735
± 1.157	19.202	±1.123	13.708	±1.136	19.407	±1.164	18.076
± 0.613	6.716	±0.613	6.705	±0.613	6.717	±0.613	6.722

technique in [17] and [18] from the frequency vector:

$$f = \begin{bmatrix} 0.01:0.01:0.09 & 0.1:0.1:0.9 & 1:0.1:3 & 3.1:1:10 \end{bmatrix} \quad (31)$$

where f comprises a range of 0.01 to 10.0 Hz and contains 46 positive frequency points. In addition, the same energy criterion (30) with a setting of 99% is used for selecting the singular values through the LBFI method, emphasizing the precision of the identified model. Furthermore, the Matlab functions ***reducespec.m*** and ***getrom.m*** are used to obtain a balanced realization of this linear model and reduce its order to $r = 9$ using BT starting from the analytical linear model obtained by PST. By applying the LBFI method, a model of order $r = 13$ is obtained. For comparison purposes, a small-signal analysis is conducted by employing the analytical model, the reduced model of order $r = 9$ from BT, and the models identified by the QBBT and LBFI approaches.

As shown in Table V, the eigenvalues of the linearized model of the KRK power system consist of two local oscillation modes at 1.1573 Hz and 1.1777 Hz, and an inter-area oscillation mode at 0.6128 Hz. The system is stable for the operating condition in which the linear model is obtained, as the real parts of the eigenvalues are negative. The modal parameters obtained from the identified models demonstrate the ability of these methods to preserve the oscillatory dynamics.

To make a more rigorous comparison, the absolute error of the models' frequency responses using BT, and the models identified by QBBT and LBFI are shown in Fig. 6 in a frequency range from 0 to 3.0 Hz. Notice that the absolute error is always greater for the model identified by the LBFI method compared to the others with errors ranging from 1.00×10^{-2} to 1.00×10^{-1} dB. For these four output/input relationships, QBBT presents a maximum error of 2.00×10^{-3} dB that can be seen in Fig. 6 a) for output 1/input 1. Furthermore, the error associated with the QBBT approach is similar to that associated with BT for the 4-output/input relationships.

B. New England Transmission System / New York Power System

The second case study selected to illustrate the QBBT application is the well-known NETS-NYPS, which is an equivalent representation of the New England/New York interconnected system [31], [41], [42], as can be seen in Fig. 7. Various studies of coherency and control of small signal oscillations have been developed from this equivalent representation. The NETS-NYPS has 16 generators and 68 buses interconnected through 86 transmission lines. Due to a large number of physical elements, it is considered a complex power system and therefore useful for QBBT evaluation.

TABLE VI
NETS-NYPS DIMENSION OF MATRICES FOR CASE f) AND $E_{th} = 98\%$

Interpolating matrices		Model matrices		
$\tilde{\mathbb{L}} \in \mathbb{C}^{5040\times960}$	$\tilde{\mathbb{M}} \in \mathbb{C}^{5040\times960}$	$\tilde{\mathbf{E}}_r \in \mathbb{R}^{29\times29}$	$\tilde{\mathbf{A}}_r \in \mathbb{R}^{29\times29}$	$\tilde{\mathbf{B}}_r \in \mathbb{R}^{29\times16}$
$\tilde{\mathbb{H}} \in \mathbb{C}^{5040\times16}$	$\tilde{\mathbb{G}} \in \mathbb{C}^{84\times960}$	$\tilde{\mathbf{C}}_r \in \mathbb{R}^{84\times29}$	$\tilde{\mathbf{D}}_r \in \mathbb{R}^{84\times16}$	

Based on the procedure proposed in Fig. 3 and according to the BCC quadrature rule adjustments presented in Table II, the identification process of the NETS-NYPS is carried out for these test cases. The analytical representation of this system is also obtained using the function ***svmgen.m*** in PST.

For this system, the smallest errors are obtained for case f) with the energy adjustment of 98%, reaching an order model of $r = 29$. Then, the dimensions of the interpolation matrices and the linear model are shown in Table VI.

The dimensions of the interpolating matrices and the model matrices obtained via the QBBT method correspond to 16 inputs of the NETS-NYPS and 84 outputs, as well as 60 quadrature points for each Gramian approximation. For this BCC quadrature adjustment, an order model of 29 is obtained, as can also be seen in Table VI. Fig. 8 compares the frequency response of the identified model for the case f) and the analytical representation of the NETS-NYPS for 4 outputs and 4 inputs of the system from 0 to 3.0 Hz.

Figs. 8 a)-d) show how the identified model manages to preserve all the oscillatory dynamics of the system. The greatest differences can be seen in magnitude in Figs. 8 a) and d), but no regarding frequency.

A reduced linear model of order $r = 29$ is obtained using BT from the NETS-NYPS analytical linear model, and a linear model of this system is also identified from the LBFI method to the frequency vector shown in (31) with the energy criterion set to 99%, allowing the analysis of oscillation modes between these four representations. The frequencies and damping ratios of these 4 linear models are presented in Table VII focusing the study on the frequency range from 0 to 1.5 Hz by the large-scale to the NETS-NYPS.

As shown in Table VII, three inter-area oscillation modes

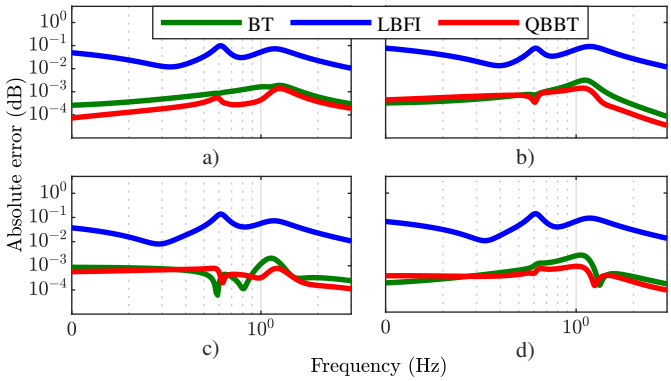

Fig. 6. Comparing the absolute error of frequency responses between BT, LBFI, and QBBT for 4-outputs and 4-inputs in the KRK power system: a) output 1/input 1; b) output 2/input 2; c) output 3/input 3; d) output 4/input 4.

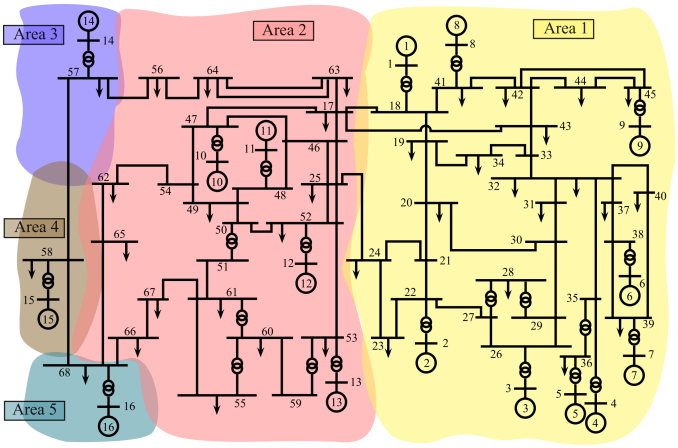

Fig. 7. New England transmission system / New York power system.

and eight local oscillation modes appear in the NETS-NYPS analytical model in the mentioned frequency range. Furthermore, the system is stable for the operating condition. For this case study, both the QBBT and LBFI methods manage to retain these oscillatory dynamics. The largest absolute error regarding frequency is 2.00×10^{-2} Hz and is found in the model identified by the LBFI method for the local oscillation mode at 1.3374 Hz. The largest absolute error associated with the damping ratio is 7.33×10^{-1} % and corresponds to the model obtained by the QBBT approach for the local oscillation mode at 1.2201 Hz. Regarding the reduced model obtained by applying BT, the frequencies and damping ratios are captured with great precision, except the damping ratio associated with the frequency oscillation mode at 0.788 Hz. It is important to highlight that BT is a technique aimed at reducing order models, providing accurate representations for the overall frequency range. On the other hand, for the reduced model obtained by the ERA method, the largest absolute error is associated with the damping ratio corresponding to the 0.788 Hz mode. In general, the frequencies and damping ratios are captured with great precision.

The absolute error associated with the frequency responses in the model identified by the QBBT approach is lower than in the models obtained by the LBFI method, as can be seen in Fig. 9 a)-d). In Fig. 9 a), an intercept between the two errors is observed for frequencies less than 1.0 Hz, but for the rest of the frequency range, the error introduced by the LBFI approach is still greater. Comparing the error associated with the QBBT method against the BT in the frequency range analyzed, a similar behavior is observed in all cases around the 1.00×10^{-3} dB. The model identified through the QBBT approach has an absolute error similar to that obtained through BT.

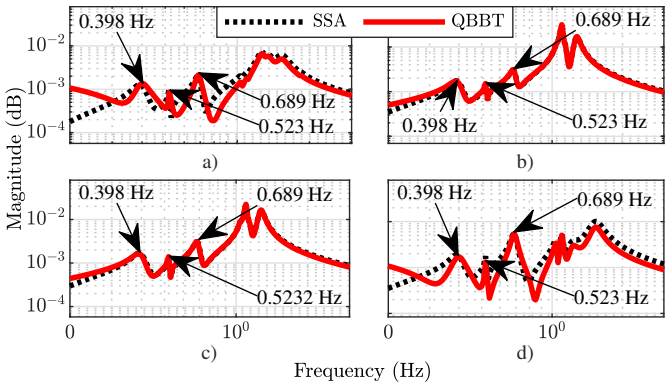

Fig. 8. Comparisons of frequency responses between SSA and QBBT for 4-outputs and 4-inputs in the NETS-NYPS: a) output 1/input 1; b) output 2/input 2; c) output 3/input 3; d) output 4/input 4.

TABLE VII
INTER-AREA OSCILLATING MODES OF THE NETS-NYPS

SSA		BT		ERA		LBFI		QBBT	
Freq. (Hz)	D.r. (%)	Freq. (Hz)	D.r. (%)	Freq. (Hz)	D.r. (%)	Freq. (Hz)	D.r. (%)	Freq. (Hz)	D.r. (%)
±0.788	3.754	±0.766	15.812	0.705	6.660	±0.788	3.629	±0.783	3.727
±0.689	2.839	±0.689	2.769	0.658	2.600	±0.689	2.887	±0.689	2.731
±0.523	0.517	±0.523	0.515	0.523	0.561	±0.523	0.533	±0.523	0.519
±0.398	6.308	±0.394	6.906	0.396	6.287	±0.398	6.402	±0.398	6.256

C. North-Eastern Power Coordination Council

The third test system used to illustrate the QBBT approach is the 48-machine Northeast Energy Coordinating Council (NPCC) system [43]. The NPCC is an expansion of the NETS-NYPS, in which the New York area is modeled in more detail. It is made up of 48 generators, 140 buses, and 232 transmission lines. Therefore, it constitutes a very useful large-scale power system to evaluate the scalability of the proposed method.

For the sake of brevity, only the modal parameters identification is presented where the proposed method is compared against the SSA and ERA techniques. Table VIII summarizes the frequencies and damping ratios obtained by SSA, ERA, and the QBBT proposed method, where seven inter-area oscillation modes appear in the NPCC analytical model. Notice that the QBBT method manages to retain these oscillatory dynamics. Therefore, the modal identification obtained by QBBT approach matches with the actual parameters provided by the SSA method, where the largest absolute error regarding frequency is 2.00×10^{-2} Hz and is found in the model identified by ERA for the inter-area oscillation mode at 0.258 Hz.

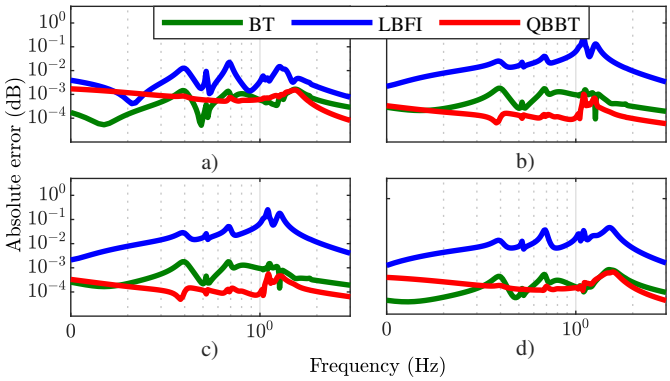

Fig. 9. Comparisons of absolute error of frequency response between BT, LBFI, and QBBT for 4-outputs and 4-inputs in the NETS-NYPS: a) output 1/input 1; b) output 2/input 2; c) output 3/input 3; d) output 4/input 4.

TABLE VIII
INTER-AREA OSCILLATING MODES OF THE NPCC SYSTEM

SSA		ERA		QBBT	
Frequency (Hz)	Damp. ratio (%)	Frequency (Hz)	Damp. ratio (%)	Frequency (Hz)	Damp. ratio (%)
0.888	3.802	0.889	0.743	0.888	2.742
0.786	6.211	0.787	6.313	0.783	5.839
0.704	6.733	0.688	6.035	0.700	6.411
0.534	7.163	0.530	8.261	0.532	6.302
0.459	8.106	0.471	8.882	0.459	8.264
0.385	10.644	0.377	14.132	0.386	10.106
0.258	16.177	0.230	27.086	0.258	16.684

On the other hand, the largest absolute error associated with the damping ratio is 10.909 % and corresponds to the ERA method for the same inter-area mode.

V. DISCUSSION

The identification of power system linear models has been successfully carried out by using the output-input dataset that, in turn, is processed by the QBBT approach. The identified linear models from the KRK test system, the NETS-NYPS, and the NPCC system manage to retain their oscillatory dynamics and could be used to adjust controllers to dampen these dynamics, as well as to carry out a coherent analysis.

To introduce the QBBT technique to power systems, the correct adjustment of the BCC quadrature rule is required for a range of frequencies in which the oscillatory modes are of interest. The error introduced into the linear representations obtained is directly determined by the adjustment of the quadrature rule, which is nothing more than the selection of the number of points for the Gramian approximations and the selection of the truncation constants.

Regarding the analytical models of the case studies, the identification of linear models in power systems using the QBBT approach is achieved with a significant order reduction, even greater than that obtained when applying the LBFI technique. Besides the error quantified is lower for the QBBT method, the new formulation makes up a useful technique for subsequent studies based on these linear representations.

VI. CONCLUSIONS

In this paper, a novel QBBT formulation, based on Gramian approximations and directional frequency data-set interpolation, is introduced in power systems. Linear models are identified for the KRK power systems, the NETS-NYPS, and the NPCC system, using frequency data extracted under the BCC quadrature rule and performing transient simulations.

The linear models obtained through the QBBT method were validated with analytical models of power systems attending to the error in the frequency response of these representations. Several adjustments of the BCC quadrature rule were analyzed to ensure a balance between the error and order of the identified models. The novel formulation was compared with the LBFI method in power systems demonstrating more accuracy in the identified models.

For the identification of power system linear models from data, the QBBT method allowed us to obtain reduced representations in the analyzed systems, preserving the precision of the BT technique, and demonstrating the performance of our proposal to be a useful technique for subsequent model-based studies in power systems.

Given the reduced order model and the proposed frequency range, the QBBT technique presents as main drawback the loss of information, as any other reduction techniques, and the resulting QBBT-based model is valid for around the operating condition in which the model is identified.

As future works, this investigation is targeted to be tested in real-time environments, where probing signals are used to stimulate the system via analog inputs and reference changes, and the measured outputs can capture the system response via analog outputs.

REFERENCES

[1] X.-F. Wang, Y. Song, and M. Irving, *Modern power systems analysis*. Springer Science & Business Media, 2010.

[2] P. S. Kundur, N. J. Balu, and M. G. Lauby, "Power system dynamics and stability," *Power system stability and control*, vol. 3, pp. 700–701, 2017.

[3] N. Hatziargyriou, J. Milanovic, and et al., "Definition and classification of power system stability–revisited & extended," *IEEE Trans. Power Systems*, vol. 36, no. 4, pp. 3271–3281, 2020, doi: 10.1109/TPWRS.2020.3041774.

[4] P. Kundur, *Power system stability*. CRC Press New York, 2007, vol. 10.

[5] P. W. Sauer, M. A. Pai, and J. H. Chow, *Power system dynamics and stability: with synchrophasor measurement and power system toolbox*. John Wiley & Sons, 2017, ch. 8.

[6] J. H. Chow and J. J. Sanchez-Gasca, *Power system modeling, computation, and control*. John Wiley & Sons, 2020, ch. 6.

[7] P. Kundur and L. Wang, "Small signal stability analysis: experiences, achievements, and challenges," in *Proceedings. Intern. Conference on Power System Technology*, vol. 1, 2002, pp. 6–12, doi: 10.1109/ICPST.2002.1053494.

[8] B. Moore, "Principal component analysis in linear systems: Controllability, observability, and model reduction," *IEEE Trans. automatic control*, vol. 26, no. 1, pp. 17–32, 1981, doi: 10.1109/TAC.1981.1102568.

[9] F. D. Freitas, J. Rommes, and N. Martins, "Gramian-based reduction method applied to large sparse power system descriptor models," *IEEE Trans. Power Systems*, vol. 23, no. 3, pp. 1258–1270, 2008, doi: 10.1109/TPWRS.2008.926693.

[10] J. W. Pierre, D. Trudnowski, and et al., "Overview of system identification for power systems from measured responses," *IFAC Proceedings Volumes*, vol. 45, no. 16, pp. 989–1000, 2012, doi: https://doi.org/10.3182/20120711-3-BE-2027.00412.

[11] N. Zhou, J. W. Pierre, and J. F. Hauer, "Initial results in power system identification from injected probing signals using a subspace method," *IEEE Trans. power systems*, vol. 21, no. 3, pp. 1296–1302, 2006, doi: 10.1109/TPWRS.2006.879292.

[12] R. Chakraborty, H. Jain, and et al., "A review of active probing-based system identification techniques with applications in power systems," *Intern. J. of Electrical Power & Energy Systems*, vol. 140, p. 108008, 2022, doi: https://doi.org/10.1016/j.ijepes.2022.108008.

[13] J. Sanchez-Gasca, D. Trudnowski, and et al., "Identification of electromechanical modes in power systems," in *IEEE Task Force Report, Special Publication TP462*, 2012, doi: 10.17023/2nn1-tn85.

[14] G. E. Mejia-Ruiz, M. R. A. Paternina, and et al., "Real-time co-simulation of transmission and distribution networks integrated with distributed energy resources for frequency and voltage support," *Applied Energy*, vol. 347, p. 121046, 2023, doi: https://doi.org/10.1016/j.apenergy.2023.121046.

[15] A. Mayo and A. Antoulas, "A framework for the solution of the generalized realization problem," *Linear algebra and its applications*, vol. 425, no. 2-3, pp. 634–662, 2007, doi: https://doi.org/10.1016/j.laa.2007.03.008.

[16] G. Gurrala, "Loewner matrix approach for modelling fdnes of power systems," *Electric Power Systems Research*, vol. 125, pp. 116–123, 2015, doi: https://doi.org/10.1016/j.epsr.2015.03.016.

[17] C. Rergis, I. Kamwa, and et al, "A loewner interpolation method for power system identification and order reduction," *IEEE Trans. Power Systems*, vol. 34, no. 3, pp. 1834–1844, 2018, doi: 10.1109/TPWRS.2018.2884655.

[18] F. Zelaya-A, J. H. Chow, and et al., "Data-driven power system linear model identification for selective modal analysis by frequency interpolations," *IET Generation, Transmission & Distribution*, vol. 15, no. 6, pp. 1107–1121, 2021, doi: https://doi.org/10.1049/gtd2.12084.

[19] A. Almunif, L. Fan, and Z. Miao, "A tutorial on data-driven eigenvalue identification: Prony analysis, matrix pencil, and eigensystem realization algorithm," *Intern. Trans. Electrical Energy Systems*, vol. 30, no. 4, p. e12283, 2020, doi: https://doi.org/10.1002/2050-7038.12283.

[20] M. L. Crow and A. Singh, "The matrix pencil for power system modal extraction," *IEEE Trans. Power Systems*, vol. 20, no. 1, pp. 501–502, 2005, doi: 10.1109/TPWRS.2004.841158.

[21] J.-N. Juang and R. S. Pappa, "An eigensystem realization algorithm for modal parameter identification and model reduction," *Journal of guidance, control, and dynamics*, vol. 8, no. 5, pp. 620–627, 1985, doi: https://doi.org/10.2514/3.20031.

[22] C. F. Van Loan and G. H. Golub, *Matrix computations*. Johns Hopkins University Press Baltimore, 1983, vol. 3.

[23] J. Moreno-Corbea, M. Paternina, and et al., "On-line system identification of power system linear models," in *2023 IEEE Power & Energy Society General Meeting (PESGM)*, 2023, pp. 1–5, doi: 10.1109/PESGM52003.2023.10252494.

[24] H. Ma, D. Yang, and et al., "Power system equivalent inertia estimation method using system identification," in *IEEE 5th Intern. Conf. on Electron. Tech. (ICET)*, 2022, pp. 360–365, doi: 10.1109/ICET55676.2022.9824227.

[25] I. V. Gosea, S. Gugercin, and C. Beattie, "Data-driven balancing of linear dynamical systems," *SIAM Journal on Scientific Computing*, vol. 44, no. 1, pp. A554–A582, 2022, doi: https://doi.org/10.1137/21M1411081.

[26] A. Morched, B. Gustavsen, and M. Tartibi, "A universal model for accurate calculation of electromagnetic transients on overhead lines and underground cables," *IEEE Trans. Power Delivery*, vol. 14, no. 3, pp. 1032–1038, 1999, doi: 10.1109/61.772350.

[27] B. Gustavsen and A. Semlyen, "A robust approach for system identification in the frequency domain," *IEEE Trans. power delivery*, vol. 19, no. 3, pp. 1167–1173, 2004, doi: 10.1109/TPWRD.2003.822530.

[28] B. Gustavsen, "Wide band modeling of power transformers," *IEEE Trans. Power Delivery*, vol. 19, no. 1, pp. 414–422, 2004, doi: 10.1109/TPWRD.2003.820197.

[29] M. Dehghani and S. K. Y. Nikravesh, "State-space model parameter identification in large-scale power systems," *IEEE Trans. Power Systems*, vol. 23, no. 3, pp. 1449–1457, 2008, doi: 10.1109/TPWRS.2008.922632.

[30] M. R. A. Paternina, C. Castrillón-Franco, and et al., "Enhancing wide-area damping controllers via data-assisted power system linear models," *Electric Power Systems Research*, vol. 217, p. 109085, 2023, doi: https://doi.org/10.1016/j.epsr.2022.109085.

[31] J. H. Chow, *Power system coherency and model reduction*. Springer, 2013, vol. 84.

[32] N. Sarkar, K. Rao, and K. Shubhanga, "A comparative study between prony and eigensystem realization algorithm for identification of electromechanical modes," in *2018 20th national power systems conference (NPSC)*, 2018, pp. 1–6, doi: 10.1109/NPSC.2018.8771722.

[33] S. Ghosh and N. Senroy, "Balanced truncation approach to power system model order reduction," *Electric Power Components and Systems*, vol. 41, no. 8, pp. 747–764, 2013, doi: https://doi.org/10.1080/15325008.2013.769031.

[34] S. K. Suman and A. Kumar, "Model reduction of power system by modified balanced truncation method," *Univers. J. Control Autom*, vol. 8, no. 3, pp. 41–52, 2020, doi: 10.13189/ujca.2020.080301.

[35] C. E. Grosch and S. A. Orszag, "Numerical solution of problems in unbounded regions: coordinate transforms," *Journal of Computational Physics*, vol. 25, no. 3, pp. 273–295, 1977, doi: https://doi.org/10.1016/0021-9991(77)90102-4.

[36] J. P. Boyd, "The optimization of convergence for chebyshev polynomial methods in an unbounded domain," *Journal of computational physics*, vol. 45, no. 1, pp. 43–79, 1982, doi: https://doi.org/10.1016/0021-9991(82)90102-4.

[37] ——, "Exponentially convergent fourier-chebshev quadrature schemes on bounded and infinite intervals," *Journal of scientific computing*, vol. 2, pp. 99–109, 1987, doi: https://doi.org/10.1007/BF01061480.

[38] G. Strang, *Linear algebra and its applications*, 2012.

[39] P. S. Kundur and O. P. Malik, *Power system stability and control*. McGraw-Hill Education, 2022.

[40] J. H. Chow and K. W. Cheung, "A toolbox for power system dynamics and control engineering education and research," *IEEE Trans. Power Systems*, vol. 7, no. 4, pp. 1559–1564, 1992, doi: 10.1109/59.207380.

[41] M. Jonsson, M. Begovic, and J. Daalder, "A new method suitable for real-time generator coherency determination," *IEEE Trans. Power Systems*, vol. 19, no. 3, pp. 1473–1482, 2004, doi: 10.1109/TPWRS.2004.826799.

[42] H. Min and E. Mallada, "Spectral clustering and model reduction for weakly-connected coherent network systems," in *2023 American Control Conference (ACC)*, 2023, pp. 2957–2962, doi: 10.23919/ACC55779.2023.10156212.

[43] M. R. Arrieta Paternina, A. Zamora-Mendez, J. Ortiz-Bejar, J. H. Chow, and J. M. Ramirez, "Identification of coherent trajectories by modal characteristics and hierarchical agglomerative clustering," *Electric Power Systems Research*, vol. 158, pp. 170–183, 2018, doi: https://doi.org/10.1016/j.epsr.2017.12.029.

Mario R. Arrieta Paternina (Member IEEE) holds a B.Eng. and M.Eng. in Electrical Engineering from National University of Colombia, Medellin, Colombia, in 2007 and 2009, respectively. In 2017, he obtained his D.Sc. degree in Electrical Engineering from CINVESTAV, and he joined the Department of Electrical Engineering at the UNAM.

José A. Moreno Corbea (Student member IEEE) received the B.S. degree in electrical engineering from the Central University Marta Abreu of "Las Villas", Cuba, in 2017. He received the M.Sc. degree in electrical engineering from the UNAM in 2023. He is currently working toward the Ph.D. degree.

Juan M. Ramirez-Arredondo (Member, IEEE) received the Ph.D. degree in electrical engineering from UANL-Mexico, San Nicolas de los Garza, Mexico, in 1992. He joined the Department of Electrical Engineering, CINVESTAV Guadalajara, Mexico, in 1999, where he is currently a full-time Professor. His research interests include smart grids, microgrids, and power electronics applications. Dr. Ramirez is a member of the Mexican Research System.

Joe H. Chow (F'92) received his MS and PhD degrees from the University of Illinois, Urbana-Champaign. After working in the General Electric Power System business in Schenectady, he joined Rensselaer Polytechnic Institute in 1987. He is an Institute Professor Emeritus and Senior Research Scientist at the Electrical, Computer, and Systems Engineering, Rensselaer Polytechnic Institute, Troy, New York, USA. His research interests include multivariable control, power system dynamics and control, voltage-sourced converter-based FACTS Controllers, and synchronized phasor data.

Alejandro Zamora-Méndez (M' 11) received his B.S. and M.Sc. in Electrical Engineering from Universidad Michoacana de San Nicolas de Hidalgo (UMSNH), Morelia, Mexico, in 2005 and 2008, respectively. He joined the Electrical Engineering Faculty, UMSNH in 2008. He received a D.Sc. degree in Electrical Engineering from CINVESTAV-Guadalajara in 2016.